NJC

Accepted Manuscript

This article can be cited before page numbers have been issued, to do this please use: V. Lippolis, R. Montis, F. Isaia, M. Arca, A. Pintus, M. C. Aragoni, A. J. Blake, F. Demartin, S. Thurow, C. Castellano, A. E. O'Connor, G. Perin and E. J. Lenardao, *New J. Chem.*, 2018, DOI: 10.1039/C8NJ00495A.

ROYAL SOCIETY OF CHEMISTRY

rsc.li/njc

View Article Online
DOI: 10.1039/C8NJ00495A

Journal Name
RSCPublishing

ARTICLE

Cite this: DOI: 10.1039/x0xx00000x

Received 00th January 2012,
Accepted 00th January 2012

DOI: 10.1039/x0xx00000x

www.rsc.org/

Structural diversity in the products formed by the reactions of 2-arylselanyl pyridine derivatives and dihalogens†

Riccardo Montis,[a] Massimiliano Arca,[a] M. Carla Aragoni,[a,*] Alexander J. Blake,[b] Carlo Castellano,[c] Francesco Demartin,[c] Francesco Isaia,[a] Vito Lippolis,[a,*] Anna Pintus,[a] Eder J. Lenardão,[d] Gelson Perin,[d] Alice E. O'Connor,[b] Samuel Thurow[d]

The reactivity of the 2-arylselanyl pyridine derivatives **L1–L4** towards dihalogens X_2 (X = I, Br) and interhalogens IX (X = Cl, Br) was studied in $CHCl_3$ or MeCN. The solid products obtained were structurally characterized and their nature points out the preference for CT spoke adducts and for seesaw insertion adducts to be formed at the N-donor and Se-donor site, respectively. DFT calculations were performed to provide a rationale for the structural diversity observed in the products obtained.

Introduction

It is well known that the reactions of molecules containing pnicogen, (mainly nitrogen and phosphorous) and chalcogen (mainly sulfur and selenium) donor atoms with homonuclear dihalogens X_2, (X = I, Br, Cl), and heteronuclear interhalogens IX (X = Cl, Br) can afford a large variety of products whose formation is not easily predictable since it depends on the nature of the donor atom (including its chemical environment) and the experimental conditions used: polarity of the solvent, reactant molar ratios, acid-base strength of the starting materials.[1-6]

In fact, the reactions of dihalogens and interhalogens with diorgano sulfur and selenium compounds (R_2E, E = S, Se) generally afford either Charge Transfer (CT) spoke adducts or seesaw- or T-shaped insertion adducts.[1-7] CT spoke adducts featuring a linear D–X–Y three body system (D = donor atom, X, Y = halogen atoms), represent an important and extensively investigated class of compounds due to their potential biological relevance and pharmacological activities (especially those formed by chalcogen donor molecules), particularly for their involvement in the mechanism of action of anti-thyroid drugs.[8, 9] In addition, oxidation products such as di-chalcogenide cations $[(R)E{-}E(R)]^{n+}$ (R = organic framework; E = S, Se; n = 1, 2) featuring a chalcogen-chalcogen bond or halonium complex cations $[(R)E{-}I{-}E(R)]^{+}$ (E = S, Se) featuring an almost linear E─I─E framework, balanced by polyhalides of different complexity, can also be formed.[1,2,9]

On the other hand, nitrogen donor molecules, especially pyridine derivatives (Py), when reacted with halogens or interhalogens can afford CT adducts of different structural complexity,[10, 11] but can also lead to ionic species, such as $(Py{-}I)^+$ cations, derived from the breaking of the I─X bond, or pyridinium $(PyH)^+$ cations counterbalanced by discrete or extended[12-14] polyhalide anions.[15]

The simultaneous presence in the donor molecule of both nitrogen-heterocyclic and chalcogen donor sites should enlarge, at least in principle, the number of products accessible by reaction with dihalogen or interhalogen acceptors. We, therefore, decided to investigate the reactions of homonuclear dihalogens X_2 (X = I, Br) and heteronuclear interhalogens IX (X = Cl, Br) with the 2-arylselanyl pyridine derivatives **L1**–**L4** containing both Se- and N-donor atoms in their molecular structure (Scheme 1) in order to establish how the difference in the reactivity of nitrogen and selenium donor atoms towards dihalogens can influence the nature of the final products.

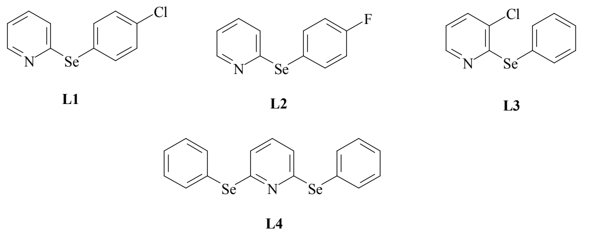

Scheme 1. Schematic representation of the 2-arylselanyl pyridines considered in this study.

Results and discussion

Synthesis and structural analysis. Information about the reactivity of donor molecules with concurrent chalcogen and pnicogen donor sites towards dihalogens X_2 (X = I, Br) and interhalogens IX (X = Cl, Br) are not reported in the literature. In the search for suitable donor molecules having both type of

View Article Online
DOI: 10.1039/C8NJ00495A

heteroatoms, we considered pyridine derivatives, for which there has been a renewed synthetic interest in the last past years due to their potential biological and pharmaceutical applications.[16] With the aim of identifying any preference in the nature of the final products, we undertook a systematic study on the reactivity of 2-arylselanyl pyridine derivatives **L1**-**L4** (Scheme 1) and dihalogens/interhalogens as a study case.

In Scheme 2, the results obtained from the reactions of **L1** with I_2, Br_2, ICl and IBr are summarized. The reactions were performed by mixing equivalent amounts of **L1** and the suitable X_2 (X = Br, I) or IX (Cl, Br) species in $CHCl_3$. All the reactions yielded 1:1 CT N-adducts of formulation **L1**·IX (X = Cl, Br, I) that were isolated and structurally characterized; only in the case of the reaction with Br_2 we were unable to isolate solid products, neither after slow evaporation of $CHCl_3$ nor by recrystallization from other solvents, due to the formation of oils and laques. The CT adducts **L1**·I_2, **L1**·IBr, and **L1**·ICl crystallize in the same space-group (triclinic) and are isomorphous (Table S1 in the ESI[†]).

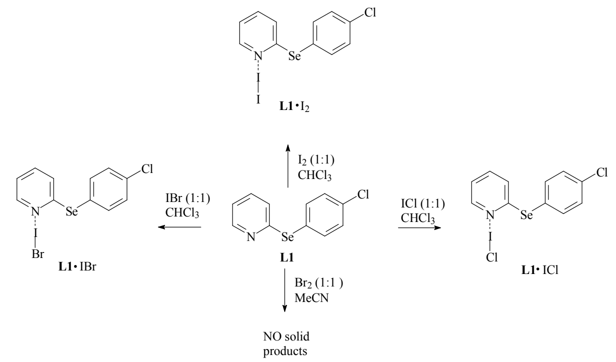

Scheme 2. Schematic representation of the compounds obtained from the reaction of **L1** with I_2, Br_2, ICl and IBr.

In all three structures, the acceptor molecule interacts with the N-donor atom of the ligand *via* an almost linear N···I–X (X = Cl, Br, I) halogen bond resulting from the interaction between the HOMO of the heterocyclic nitrogen atom and the σ* LUMO of the acceptor (Fig. 1a-c).

The N···I distances [2.497(3), 2.410(3) and 2.368(2) Å for **L1**·I_2, **L1**·IBr, and **L1**·ICl, respectively] decrease on increasing the electronegativity of X. This is in agreement with the structural data found in the Cambridge Structural Database (CSD) for similar Py···I–X (X = Cl, Br, I) 1:1 CT adducts that show N···I distances falling in the range 2.25-2.98 Å with the shortest values always observed for X = Cl. The I—X bond lengths are 2.7631(9), 2.6229(9), and 2.5311(9) Å for **L1**·I_2, **L1**·IBr, and **L1**·ICl, respectively and result elongated (from 4 to 9%) if compared with the corresponding I—X bond distances measured for the free acceptors in the gas phase (I—X distances for gaseous I_2, IBr and ICl are 2.67 Å, 2.47 Å and 2.32 Å, respectively).[17] These values are in line with those reported for similar pyridine adducts in the CSD (I—X are in the ranges of 2.74-2.83, 2.59-2.65, and 2.44-2.56 Å for X = I, Br, and Cl, respectively), with an inverse relationship between the N···I and the I—X bond distances. The N···I—X halogen bond is assisted by Se···I—X weak contacts involving the Se atom of **L1** and the iodine atom of the IX (X = Cl, Br, I) molecule (Fig. 1a-c), with Se···I distances ranging from 3.35 (**L1**·ICl) to 3.50 Å (**L1**·I_2) (sum of the van der Waals radii for the Se and I atoms is 3.88 Å) and Se···I—X angles varying from 126.2° (**L1**·IBr) to 126.8° (**L1**·I_2). The substituted phenyl ring is perpendicular to the plane of the pyridine ring in all three structures.

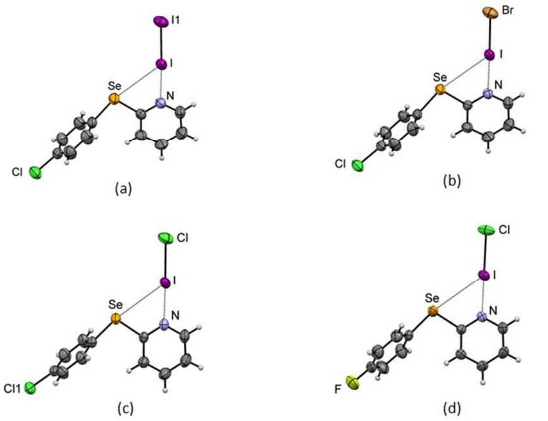

Figure 1. ORTEP view of the asymmetric unit in (a) **L1**·I_2; (b) **L1**·IBr; (c) **L1**·ICl; (d) **L2**·ICl. N···I = 2.497(3), 2.410(3), 2.368(2), 2.336(3) Å; I–X = 2.7631(9), 2.6229(9), 2.5311(9), 2.511(1) Å; N–I–X = 178.17(7), 178.74(7), 178.92(6), 179.52(7)° for **L1**·I_2, **L1**·IBr, **L1**·ICl and **L2**·ICl, respectively. Displacement ellipsoids are drawn at the 50% probability level.

The analysis of the crystal structures in **L1**·I_2, **L1**·IBr, and **L1**·ICl shows that no relevant intermolecular interactions involving the IX (X = I, Br, Cl) coordinated acceptors are observed. This is probably the reason why the different nature of the coordinated dihalogen/interhalogen species does not affect the final assembly of the resulting CT adduct units in the crystal lattices, leading to isomorphous compounds. The crystal packings in **L1**·I_2, **L1**·IBr, and **L1**·ICl show a common 2-D arrangement of molecules (Fig. 2), formed by adjacent 1-D chains of adduct units, each built *via* set of π···π interactions involving couples of parallel and partially overlapped chlorophenyl rings (interplanar distances are 3.67, 3.66, and 3.62 Å, respectively, with a slippage angle of 19° for all three compounds)[18] assisted by weak contacts such as C—H···Cl (Cl atom on the phenyl ring) or Se···π[19] with C···Se distances of 3.407(3), 3.462(4), and 3.505(4) Å, and H···Cl distances of 2.96, 2.94, and 2.99 Å for **L1**·ICl, **L1**·IBr, and **L1**·I_2, respectively, which lie just at or slightly below the sum of van der Waals radii of the relevant atoms.[20]

From the reactions of **L2** with I_2, Br_2, IBr and ICl in CH_3CN solution, crystals suitable for X-ray diffraction were obtained only for **L2**·ICl. Even if the adduct crystallizes in a different space group (monoclinic, Table S1[†]), its structural features closely resemble those found for the family of **L1**·IX CT N-adducts (X = Cl, Br, I, Fig. 1d): the N···I distance is 2.336(3) Å and falls among the lowest values within the expected range; the I—Cl distance is 2.511(1) Å. The packing of the CT adduct units in **L2**·ICl is very similar to that previously described for **L1**·IX adducts (Fig. 2c), with small differences regarding the packing of the common 2-D arrangements that are related by

View Article Online
DOI: 10.1039/C8NJ00495A

inversion symmetry in the case of the isomorphous set of CT adducts **L1**·IX (Fig. 2b), and by glide planes in the case of the adduct **L2**·ICl (Fig 2c).

The similarities found among the 1:1 CT adducts of **L1** and **L2**, drove us to attempt the co-crystallization of equivalent amounts of **L1**·I_2 and **L2**·ICl in CH_3CN, that yielded crystals corresponding to the formulation $C_{11}H_8Cl_{1.27}F_{0.32}I_{1.41}NSe$. Interestingly, single crystal X-ray diffraction analysis revealed the formation of a 1:1 CT adduct isomorphous with **L2**·ICl. The uncoordinated halogen site of the dihalogen moiety in the adduct unit shows mixed I/Cl occupancies of 0.410(5)/0.590(5), the same it is found for the halogen site on the aryl moiety of the donor molecule which shows mixed Cl/F occupancies of 0.68(2)/0.32(2), so that the adduct can be formulated as $(\mathbf{L1})_{0.68}/(\mathbf{L2})_{0.32}\cdots I{-}I_{0.41}/Cl_{0.59}$. The two bond distances in the fragment N···I—X (X = $I_{0.41}/Cl_{0.59}$) are very similar to those previously discussed for **L1**·I_2, **L1**·IBr, **L1**·ICl and **L2**·ICl: N···I 2.357(7) Å, I—X 2.686(2) Å [N—I—X = 177.7(2)°]; the I—X value is affected by the mixed nature of the coordinated di-halogen, and intermediate between those found for **L1**·I_2 and **L1**·ICl and **L2**·ICl. These findings open the possibility to obtain different polymorphs for the 1:1 CT adducts of **L1** and **L2** with dihalogens/interhalogen molecules as already observed for 1:1 I_2 and IBr CT adducts of thione-containing donor molecules.[21]

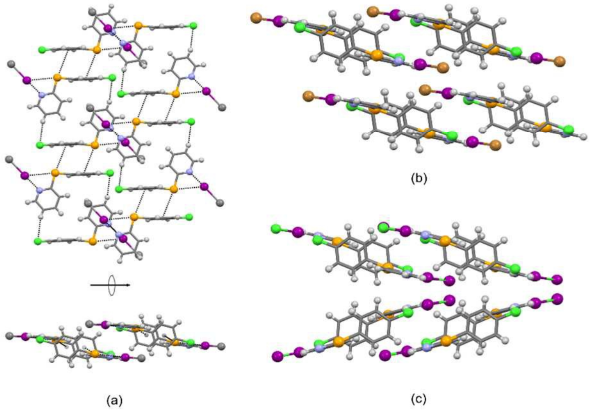

Figure 2. Crystal packing comparison for the four adducts of **L1**. (a) Common 2-D assembly viewed along two perpendicular directions. The X atom is colored as grey to represent a generic 1:1 CT adduct **L1**·IX; (b) Crystal packing of structure **L1**·IBr as representative for the set of isomorphous structures **L1**·I_2, **L1**·IBr and **L1**·ICl, viewed down the [111] direction; (c) Crystal packing of structure **L2**·ICl viewed down the [110] direction.

The isolation and characterization of new CT adducts of dihalogens and interhalogens led us to consider them in the framework of the renewed interest in such systems as potential examples of three-body systems featuring a central halogen atom[22] and therefore, halogen bonding. In fact, molecular systems displaying the D···I–X group (D = chalcogen or pnicogen atom) can be classified as cases in which halogen bonding (XB, the interaction between a polarized halogen atom and a Lewis base) formally occurs between a halogen bond donor (I–X) and a halogen bond acceptor (Lewis base containing a D donor atom).[23] The study of the chemical bond in both neutral CT adducts between X_2/IX species and chalcogen/pnicogen donors, and trihalides can, therefore, help understand the origin and nature of XB, including similarities and differences with other weak intermolecular interactions.[24-26]

Although, it is not easy to assign the contribution of each energy term to the bonding in these linear three-body systems featuring a total of 22 valence shell electrons and formed by three aligned main group elements. Both the Rundle-Pimentel model for electron-rich (3c-4e) systems,[27] and the CT model support a covalent view of the bonding and account for a total bond order of 1 in these hyper-coordinated systems, the former model fitting better for symmetric systems, the latter describing better asymmetric arrangements.

These conclusions are nicely supported by the structural features retrieved from the Cambridge Structural Database (CSD) for linear three-body systems involving either trihalogens, X–X–X (X = Br, I), or halogen(s) and chalcogen(s), E–X–Y, X–E–Y, and E–X–E (E = S, Se; X = Y = Cl, Br, I; X = I, Y = Cl, Br).[28] The relative elongations (*δ*) of the two bonds in the examined three-body systems with respect to the sum of the relevant covalent radii show a continuous variation from balanced situations to very unbalanced ones without indications of a critical distance differentiating substantially covalent from predominantly electrostatic bonds.

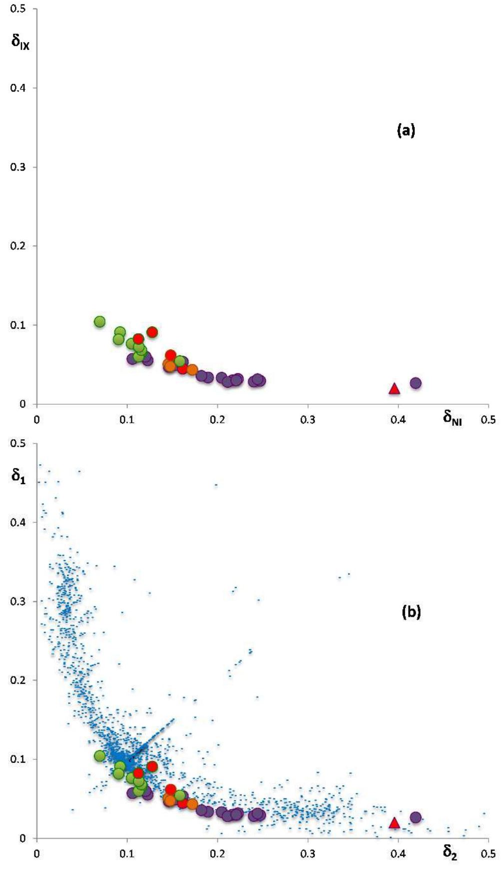

Figure 3. (a) Structural data of N···I–X (X = Cl, Br, I) fragments for **L1**·I_2, **L1**·IBr, **L1**·ICl, **L2**·ICl (red points) and pyridyl CT adducts from CSD (X = I, purple points; X = Br, orange points; X = Cl, green points) as scatter plot of δ_{IX} vs. δ_{NI}; (b) structural data of the N···I–X (X = Cl, Br, I) fragments as in (a) overlapped with those related to E–X–Y, X–E–Y, E–X–E E–X–Y, X–E–Y, and E–X–E (E = S, Se; X = Y = Cl, Br, I; X = I, Y = Cl, Br), and X–X–X (X = Br, I) from ref. 28 all depicted as blue dots. The red triangle refers to the values calculated for $(\mathbf{L4})_2$·I_2 (see below).

View Article Online
DOI: 10.1039/C8NJ00495A

Furthermore, all data can be fitted by a common nonlinear least-squares equation derived from the Bond-Valence model (BV) independently of the nature of the donor atom.[28]

Using Charge Displacement analysis, Energy Decomposition Analysis and zeroth order Symmetry Adapted Perturbation Theory, we have recently demonstrated that the specific contributions of the interacting atoms to the halogen bonding in trihalides and CT adducts of chalcogenide donors, in terms of charge transfer and electrostatic polarization, does not depend on the nature of the involved atoms, but only on their geometrical arrangement and, specifically, on the relative elongations (δ).[29]

These considerations also apply to dihalogen/interhalogen CT adducts of pyridyl donors. In fact, the relative elongations (δ) of the N···I and I—X bonds for N···I—X (X = Cl, Br, I) fragments retrieved from CSD, and those observed for **L1**·I_2, **L1**·IBr, **L1**·ICl and **L2**·ICl are as correlated as in trihalides and CT adducts of chalcogen donor molecules (Fig. 3a) and nicely fit the structural data for the other three body systems previously considered (Fig. 3b).

In an attempt to verify the effect of a different position of the halogen atom on the aromatic rings we considered the reactivity of **L3** towards dihalogens and interhalogens. Ligand **L3** differs from **L1** in the position of the Cl substituent, bound to the pyridyl ring rather than to the phenyl one (Scheme 1). Crystals suitable for X-ray diffraction were only obtained from the reaction of **L3** with IBr in CH_3CN (1:1 molar ratio) by slow evaporation of the solvent. The X-ray characterization revealed a product consistently different from those described so far, *i.e.* the triiodide salt (**L3**)(**L3**H)I_3. It crystallizes (Table S1)† as a 1:1 H-bond adduct between the free donor **L3** and the triiodide salt $(\mathbf{L3}\mathrm{H})^+I_3^-$. The asymmetric unit consists of one independent free pyridine donor **L3**, one independent protonated pyridinium cation **L3**H^+, and one independent triiodide I_3^- as a counter-ion. The analysis of the conformation shows that both **L3** and **L3**H^+ adopt the same geometry, with the phenyl ring oriented perpendicular to the pyridine/pyridinium ring but, differently from what observed in **L1**·IX (X = Cl, Br, I) CT N-adducts, the pyridine nitrogen atom point towards the phenyl ring, possibly due to the presence of the Cl substituent on the pyridyl ring. The neutral **L3** and the cationic $(\mathbf{L3}\mathrm{H})^+$ species interact to each other *via* a short N–H···N hydrogen bond [N1···H1' 2.17 Å, N1···N1' 2.796 (4) Å, N1'–H1'–N1 139.0°] (Fig. 4a). Furthermore, the neutral and protonated pyridyl rings from the H-bonded **L3** and $(\mathbf{L3}\mathrm{H})^+$, respectively, are oriented in order to $\pi\cdots\pi$ interact with the almost parallel adjacent phenyl rings from $(\mathbf{L3}\mathrm{H})^+$ and **L3** [intercentroid distances are 3.517(2) and 3.608(2) Å, with angles between planes of the interacting aromatic rings of 0.5 and 12,4°, respectively], that contribute to the cohesion of the resulting dimeric assembly. The almost linear [I1–I2–I3 176.25(1)°] and asymmetric [I1–I2 2.8702(3), I2–I3 2.9220(3) Å] I_3^- anion is anchored to the $(\mathbf{L3}\mathrm{H})^+$ cation *via* a Se1'···I1 contact of 3.6958(4) Å (sum of the van der Waals radii for Se and I is 3.88 Å) (Fig. 4a).

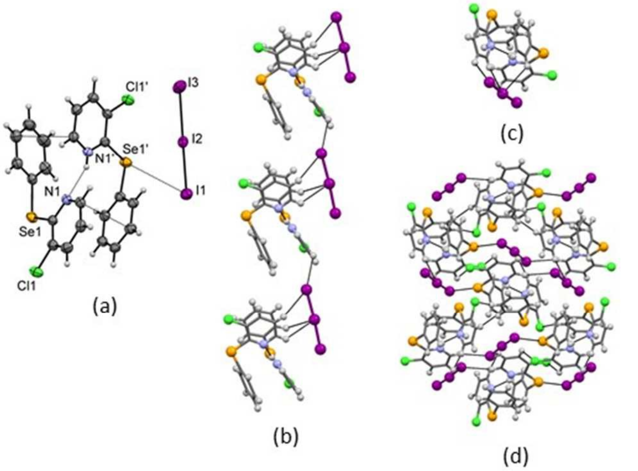

Figure 4. (a) ORTEP view of the asymmetric unit in (**L3**)(**L3**H)I_3, displacement ellipsoids are drawn at the 50% probability level, I1–I2 2.8702(3), I2–I3 2.9220(3) Å, I1–I2–I3 176.25(1)°; (b) 1-D $[\mathbf{L3}\cdot(\mathbf{L3}\mathrm{H})^+]\cdots I_3^-\cdots[\mathbf{L3}\cdot(\mathbf{L3}\mathrm{H})^+]\cdots I_3^-$ chains propagating along the axis *a* direction and viewed down the axis *b* direction; (c) 1-D $[\mathbf{L3}\cdot(\mathbf{L3}\mathrm{H})^+]\cdots I_3^-\cdots[\mathbf{L3}\cdot(\mathbf{L3}\mathrm{H})^+]\cdots I_3^-$ chains viewed down the *a* direction; (d) crystal packing of $(\mathbf{L3})(\mathbf{L3}\mathrm{H})^+I_3^-$ viewed down the axis *a* direction.

In the crystal packing, H-bonded adducts $[\mathbf{L3}\cdot(\mathbf{L3}\mathrm{H})^+]$ and I_3^- counter-ions interact parallel to the crystallographic *a* axis through C–H···I contacts (H···I distances in the range 3.09-3.18 Å), forming linear 1-D $[\mathbf{L3}\cdot(\mathbf{L3}\mathrm{H})^+]\cdots I_3^-\cdots[\mathbf{L3}\cdot(\mathbf{L3}\mathrm{H})^+]\cdots I_3^-$ chains (Fig. 4b). Adjacent 1-D chains pack along the axes *b* and *c* directions *via* weak C–H···Cl contacts involving the Cl substituents of both **L3** and $(\mathbf{L3}\mathrm{H})^+$ units (H···Cl distances are 3.03 Å and 2.96 Å respectively), along with the C–H···I, and Se···I interactions previously described (Fig. 4d) to define the crystal packing.

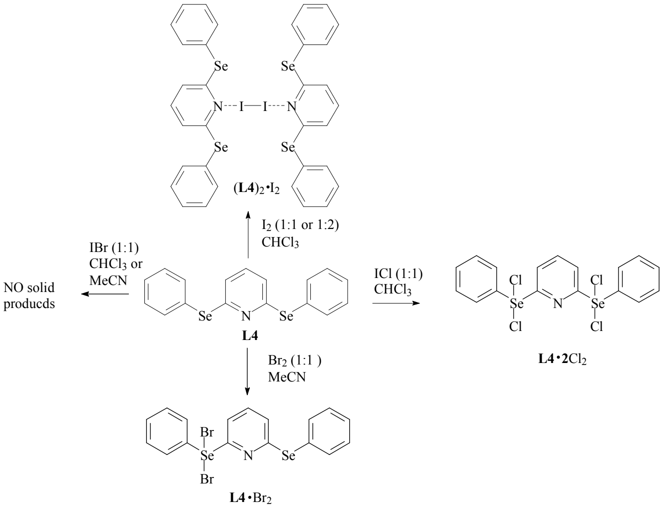

Scheme 3. Schematic representation of the compounds obtained from the reaction of **L4** with I_2, Br_2, ICl and IBr. Crystals of **L4** were isolated by slow evaporation of the solvent from the reaction mixture of **L4** and IBr in CH_3CN in 1:1 molar ratio.

Bis(phenylselanyl)pyridine (**L4**) was obtained by reacting 2,6-dichloropyridine and diphenyl diselenide at 90 °C.[16] Differently

View Article Online
DOI: 10.1039/C8NJ00495A

from **L1**–**L3**, **L4** features two phenylselanyl groups linked to the same pyridine ring in ortho positions (Scheme 1).

The reactions of **L4** with dihalogens and interhalogens are summarized in Scheme 3. It is interesting to note that, notwithstanding experimental conditions similar to those previously described for **L1**–**L3** were adopted, the insertion adducts **L4**$\cdot Br_2$ and **L4**$\cdot 2Cl_2$ were isolated from the reactions of **L4** with Br_2 and ICl in 1:1 molar ratio, respectively. The reaction of **L4** with I_2 even using a 1:2 **L4**/I_2 molar ratio, always yielded the $(\mathbf{L4})_2\cdot I_2$ CT N-adduct in which the diiodine molecule is bridging two donor units (Scheme 3, Table S1[†]).

The I_2 molecule in $(\mathbf{L4})_2\cdot I_2$ lies on an inversion center and bridges two donor molecules *via* two weak equivalent N···I**—**I halogen bonds (Fig. 5a). This adduct presents bond lengths similar to those found in the quinoxaline-disulphide adduct $(Q_2S_2\cdot I_2)_n$.[30] The N···I distance is 2.936(3) Å [N···I–I' 175.77(7)°, (' = -x, -y, -z)], significantly longer than those found in the previously examined pyridine-iodine adducts (Fig. 3a); correspondingly, the di-iodine bond is only slightly perturbed with a I**—**I' bond distance of 2.722(1) Å, which is very similar to that found in pure diiodine in the solid state [2.715 (6) Å].[31] As in the case of **L1**$\cdot I_2$, **L1**$\cdot$IBr, **L1**$\cdot$ICl and **L2**$\cdot$ICl, weak Se···I contacts of 3.6661(9) and 3.7165(9) Å from the Se1 and Se2 atoms of **L4**, respectively [Se1···I–I' 133.14(2), Se2···I–I' 132.79(3)°], support the N···I–I···N halogen bonds. The structural data of the N···I–I···N nicely fit the distribution of the structural data in Figure 3a.

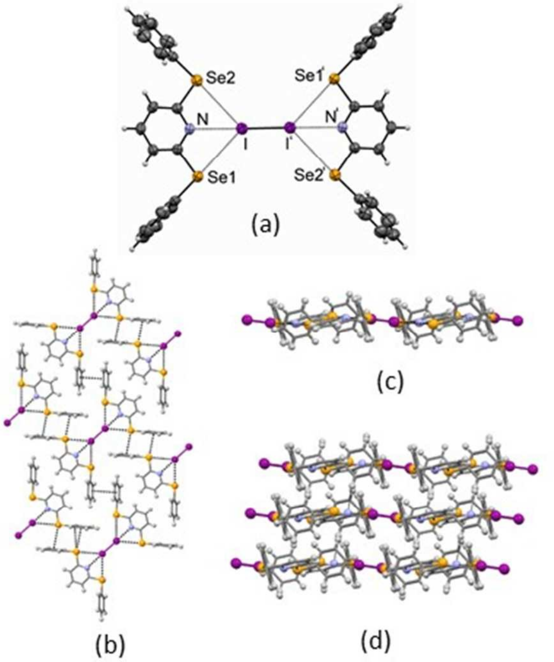

Figure 5. (a) ORTEP view of the bridging adduct unit in $(\mathbf{L4})_2\cdot I_2$, displacement ellipsoids are drawn at the 50% probability level, ' = -x, -y, -z; (b) 2-D array of interacting $(\mathbf{L4})_2\cdot I_2$ units viewed normal to the (121) plane, and (c) along the (121) plane; (d) assembly of three instances of 2-D sheets of interacting $(\mathbf{L4})_2\cdot I_2$.

Adjacent **L4**···I–I···**L4** dimeric units interact *via* weak Se···Ar (C···Se distances is 3.55 Å) and π···π contacts (interplanar distance is 3.53 Å with a slippage angle of 21°) forming 2-D sheets parallel to the (121) plane (Fig. 5b and 5c) which stack perpendicular to the plane (121) (Fig. 5d).

By reacting equivalent amounts of **L4** with ICl or Br_2, in $CHCl_3$ and CH_3CN, respectively, solid compounds corresponding to the formulations **L4**Cl_4 and **L4**Br_2 were isolated.

Single crystal X-ray diffraction analysis revealed that in both cases the reactions involved the Se site(s) and resulted in the formation of seesaw hypervalent adducts **L4**$\cdot Br_2$ and **L4**$\cdot 2Cl_2$ (Scheme 3, Table S1[†]).

Furthermore, although both complexes were prepared by mixing **L4** and the appropriate halogen/interhalogen in 1:1 molar ratio, in the case of the reaction with ICl, insertion adduct formation was observed on both Se donor atoms, while in the reaction with Br_2, the oxidative addition reaction occurred only on one of the two available Se donors.

In **L4**$\cdot Br_2$, the almost linear [Br1–Se1–Br2 175.20(3)°] and symmetric [Se1–Br1 2.5482(10), Se1–Br2 2.5465(9) Å] Br–Se–Br three body system is tilted of 63.3° (N–C7–Se1–Br1 torsion) with respect to the plane of the pyridine ring. The phenyl rings are also tilted with respect the plane of the pyridine ring, of -41.4° (C7–Se1–C1–C6 torsion) for the ring bearing the Se atom involved in the hypervalent system, and of 96.9° (C11–Se2–C12–C17 torsion) for the other phenyl ring (Fig. 6a). The overall conformation adopted by **L4** in **L4**$\cdot Br_2$ is very similar to the conformation of free **L4** (Scheme 3, Table S1[†]), which shows the phenyl rings on the same side of the pyridine ring (Fig. 6b), with the only difference that in free **L4** the two phenyl rings are tilted of about the same angle with respect the plane of the pyridine ring (see Fig. S1 in ESI[†]).

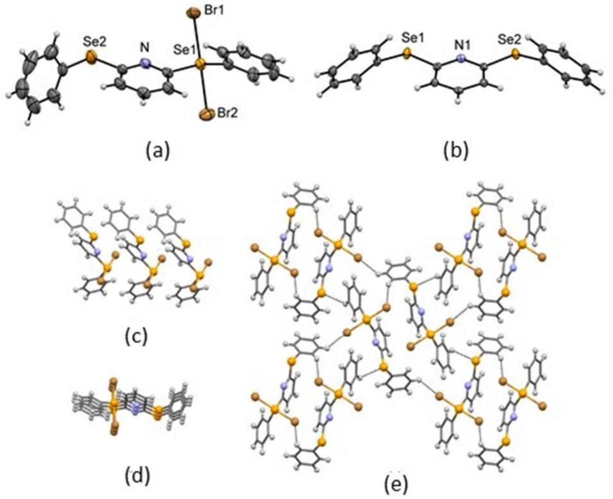

Figure 6. (a) ORTEP view of the asymmetric unit in **L4**Br_2, Se1–Br1 2.5482(10), Se1–Br2 2.5465(9) Å, Br1–Se1–Br2 175.20(3)°; (b) ORTEP view of the asymmetric unit in **L4**; (c), (d) alignment of **L4**Br_2 units along the *c* direction ; (e) 2-D sheet of interacting **L4**Br_2 units viewed down the axis *c* direction. in (a) and (b) displacement ellipsoids are drawn at the 50% probability level.

The crystal packing of **L4**$\cdot Br_2$ does not evidence relevant intermolecular interactions, and it can be described as resulting from

1-D rows formed by units of **L4**·Br_2 stacking along the axis *a* direction (Figs. 6c and 6d). 1-D rows of this kind are related by glide planes and connected along the axes *a* and *b* directions *via* weak C–H···Br (H···Br distances are 3.02 Å and 3.03 Å, respectively) and C–H···Se contacts (H···Se distance is 3.04 Å) to form 2-D corrugated sheets (Fig. 6e).

In **L4**·$2Cl_2$, both Se donor atoms undergo the oxidative addition of formally chlorine molecules, presumably deriving from disproportion of ICl. Both Cl–Se–Cl three-body systems are almost linear [Cl(11)–Se(1)–Cl(12) and Cl(21)–Se(2)–Cl(22) angles are 173.46(2)° and 173.70(2)°, respectively] and slightly asymmetric [Se(1)–Cl(11) and Se(1)–Cl(12) distances are 2.3843(6) Å and 2.3590(5) Å, respectively; Se(2)–Cl(21) and Se(2)–Cl(22) distances are 2.4471(5) Å and 2.3252(5) Å]. The conformation adopted by **L4** in **L4**·$2Cl_2$ is different from that observed in free **L4** and **L4**·Br_2: the phenyl rings are located on opposite side with respect the pyridine one, like the claws of a crab, tilted of -142.3 (2)° and 49.4(2)°, respectively (Fig. 7a).

Each independent hypervalent **L4**·$2Cl_2$ adduct is connected to adjacent ones *via* a set of three weak C–H···Cl interactions (H···Cl distances are 2.89 Å, 2.89 Å and 2.91 Å respectively), and a set of two Se···Cl interactions [Se···Cl distances are 3.5878(6) Å and 3.6406(7) Å, respectively] to form 2-D corrugated sheets (Figs. 7b and 7c) parallel to the plane (-101). Adjacent 2-D arrangements of this kind are then assembled approximately along the axis *a* direction by C–H···Cl interactions (H···Cl distance is 2.89 Å) (Fig. 7d).

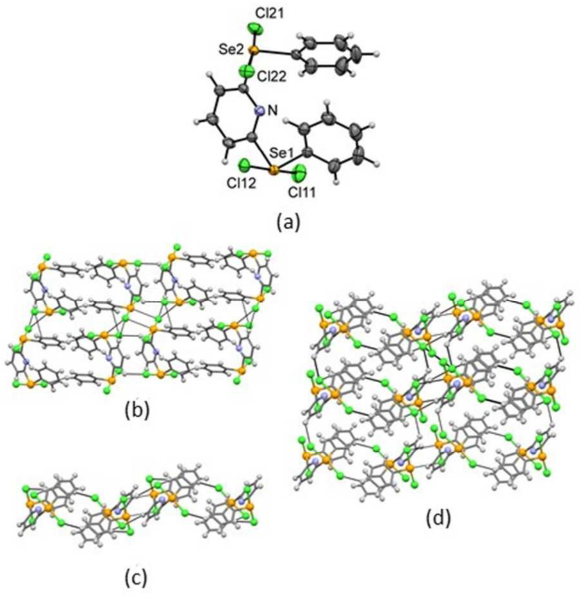

Figure 7. (a) ORTEP view of the asymmetric unit in **L4**·$2Cl_2$, Se(1)–Cl(11) 2.3843(6), Se(1)–Cl(12) 2.3590(5), Se(2)–Cl(21) 2.4471(5), Se(2)–Cl(22) 2.3252(5) Å, Cl(11)–Se(1)–Cl(12) 173.46(2), Cl(21)–Se(2)–Cl(22) 173.70(2)°, displacement ellipsoids are drawn at the 50% probability level; (b) 2-D corrugated sheet of interacting **L4**·$2Cl_2$ units viewed down the axis *a* direction; (c) 2-D sheet viewed down the axis *b* direction; (d) assembly of three instances of the 2-D sheets viewed down the axis *b* direction.

DFT Calculations. In order to account for the variety of products obtained by reacting the ligands **L1**–**L4** with dihalogens X_2 (X = Cl, Br, I) and interhalogens IX (X = Cl, Br), a computational investigation was undertaken at the density functional theory (DFT)[32] level of theory (see Experimental Section). Given the similar coordination ability shown by **L1** and **L2**, and the lack of isolated spoke or seesaw adducts in the case of **L3**, we decided to choose **L1** and **L4** as model systems. The optimized geometry of the free ligands in the gas phase (Fig. S2, Table S2 in ESI†) shows that in both **L1** and **L4** the aromatic rings lie on almost perfectly perpendicular planes (with torsion angles τ between the phenyl and pyridyl rings of 91.2 and 91.0° for **L1** and **L4**, respectively). For both ligands, the C–Se bond lengths were calculated in the range 1.924-1.926 Å, with C_{Py}–Se–C_{Ph} bond angles of 100.42 and 100.13°, respectively.

The optimized metric parameters calculated for **L4** are in perfect agreement with the structural data discussed above for the same compound. In particular, the metric parameters involving the N and Se donor atoms are calculated very precisely [optimized values: 1.924, 1.926 Å and 100.13 ° for C_{Py}–Se, C_{Ph}–Se, and C_{Py}–Se–C_{Ph}, respectively; corresponding average structural data: 1.921(3), 1.927(4) Å and 100.6(3) °]. The donor ability of **L1** and **L4** towards dihalogens and interhalogens *via* either the nitrogen or the selenium atoms is testified by the localization of Lone Pairs (LPs) of electrons on both donor sites in the Kohn-Sham occupied frontier molecular orbitals of the ligands (Fig. 8).

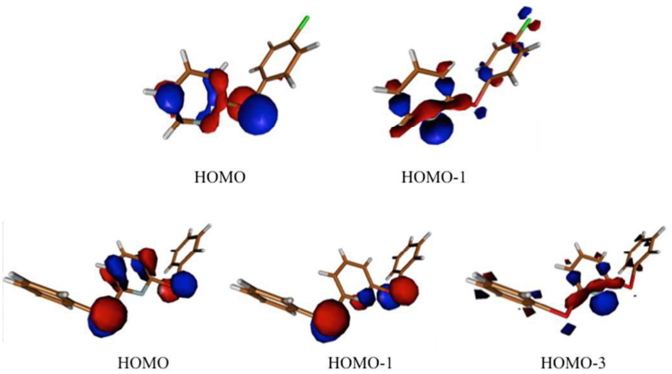

Figure 8. Isosurface drawings of selected occupied Kohn-Sham frontier molecular orbitals calculated for **L1** (top) and **L4** (bottom). Cutoff value = 0.05 |e|.

Although the LPs on the Se atoms are calculated to assume less negative eigenvalues than those on pyridine nitrogen donor atoms, the charge distribution calculated at NBO level[33] indicates a larger charge density on the pyridine nitrogen atom as compared to selenium (Q_N = -0.510 and -0.532 |e|; Q_{Se} = 0.469 and 0.470 |e| for **L1** and **L4**, respectively). In order to evaluate the different stabilities of the reaction products, both 1:1 CT spoke N/Se-adducts and 1:1 seesaw Se-adducts of **L1** and **L4** were optimized (Figs. S3-S10 and Tables S3-S8 in ESI†).

A good agreement was found between the metric parameters of the optimized structures and the corresponding structural data (namely **L1**·I_2, **L1**·ICl, **L1**·IBr, and **L4**·Br_2). Bond distances and angles differ by less than 0.15 Å and 5°, respectively, in the two sets of data, the

View Article Online
DOI: 10.1039/C8NJ00495A

most significant difference being the slight overestimation of the N–I distance by about 0.1 Å in CT N-adducts (Table S3). Based on the X-ray single crystal data discussed above, the 2:1 N-adduct $(\mathbf{L4})_2{\cdot}I_2$ and the 1:2 Se-adduct $\mathbf{L4}{\cdot}2Cl_2$ were also optimized, and again a good agreement was found with the corresponding structural data (with differences between optimized and structural bond lengths lower than 0.06 Å and angles lower than 4°; Tables S6 and S8 in ESI[†]). Remarkably, the geometry of the donor molecules in the corresponding 1:1 N-adducts does not show any significant variation in bond lengths and angles (see Tables S3 and S6 in ESI[†]) on varying the nature of the dihalogen/interhalogen species involved in the adduct formation, thus allowing for the possibility of isomorphism (see above). A comparison between the 1:1 and 2:1 N-adducts $\mathbf{L4}{\cdot}I_2$ and $(\mathbf{L4})_2{\cdot}I_2$ shows that the optimized parameters are almost identical for the two systems, only the N─I distance increasing by about 0.3 Å on passing from $\mathbf{L4}{\cdot}I_2$ to $(\mathbf{L4})_2{\cdot}I_2$ (Fig. S7 in ESI[†]). Analogously, a comparison of the metric parameters optimised for the 1:1 and the 1:2 seesaw Se-adducts of **L4** with dichlorine (see Fig. S9 and Table S8 in ESI[†]) shows only negligible differences. In order to rationalize the experimental results, the adduct formation enthalpies ΔH_f at 298.15 K of 1:1 CT spoke N- and Se-adducts, and 1:1 seesaw Se addition products were calculated (Table 1).

Table 1. Adduct formation enthalpies ΔH_f (kcal mol^{-1}) calculated for 1:1 CT spoke N- and Se-adducts and 1:1 seesaw Se-adducts **L1**·XY and **L4**·XY (X = Y = Cl, Br, I; X = I, Y = Cl, Br) at the optimized geometries.

	1:1 CT N-adducts	1:1 CT Se-adducts	1:1 seesaw Se-adducts
$\mathbf{L1}{\cdot}Cl_2$	-7.0	-6.4	-26.6
$\mathbf{L1}{\cdot}Br_2$	-9.4	-7.8	-10.8
$\mathbf{L1}{\cdot}I_2$	-9.4	-7.0	2.6
L1·ICl	-15.3	-11.5	-8.2
L1·IBr	-12.4	-9.3	-3.0
$\mathbf{L4}{\cdot}Cl_2$	-5.7	-6.8	-26.9
$\mathbf{L4}{\cdot}Br_2$	-7.8	-8.2	-11.2
$\mathbf{L4}{\cdot}I_2$	-7.3	-7.4	2.0
L4·ICl	-13.2	-12.2	-9.1
L4·IBr	-10.3	-9.9	-3.8

Although the formation of all reaction products is favoured ($\Delta H_f < 0$), the stabilities of seesaw hypercoordinated Se compounds and spoke N-adducts show opposite trends. While the formation of seesaw compounds becomes progressively more exothermic along the series I_2 > IBr > ICl > Br_2 > Cl_2, the adduct formation enthalpies of CT N-adducts follow the trend Cl_2 > Br_2 = I_2 > IBr > ICl. The reason for the decrease in the adduct formation enthalpies (and hence the increase in the stability of the corresponding adducts) along the series can be attributed largely to the increase in the donor:acceptor interaction, since a Second Order Perturbation Theory Analysis of Fock Matrix in NBO Basis shows for both **L1** and **L4** an increase in the interaction energy showing a trend roughly parallel to that calculated for ΔH_f (**L1**·XY N-adducts: 22.92, 30.19, 26.98, 35.36, and 42.78 kcal mol^{-1} for IX = Cl_2, Br_2, I_2, IBr, and ICl, respectively; **L4**·XY N-adducts: 25.39, 32.32, 26.90, 36.79, and 46.01 kcal mol^{-1} for XY = Cl_2, Br_2, I_2, IBr, and ICl, respectively). The ΔH_f values calculated for the hypothetical 1:1 CT Se-adducts are always intermediate between seesaw Se-compounds and spoke N-adducts, so that their formation is not energetically favoured in any cases but for $\mathbf{L4}{\cdot}I_2$, which features very close ΔH_f values for the charge-transfer N- and Se-adducts. Therefore, seesaw compounds are the most favoured products only when the donors are reacted with the most oxidant dichlorine and, to a much lesser extent, dibromine, while spoke N-adducts are energetically favoured in all the other cases (I_2, ICl, IBr). Accordingly, the only examples of isolated seesaw Se-adducts are represented by $\mathbf{L4}{\cdot}2Cl_2$ and $\mathbf{L4}{\cdot}Br_2$, while all the other isolated products [$\mathbf{L1}{\cdot}I_2$, **L1**·IBr, **L1**·ICl, and $(\mathbf{L4})_2{\cdot}I_2$] are N-adducts (see above). Notably, the ΔH_f value calculated for $\mathbf{L4}{\cdot}2Cl_2$ (-51.0 kcal mol^{-1}) is roughly double than that estimated for the 1:1 seesaw adduct $\mathbf{L4}{\cdot}Cl_2$ (-26.9 kcal mol^{-1}, Table 1), indicating that the oxidative addition of dichlorine occurs independently on the two phenylselanyl pendants. On the contrary, the formation enthalpies calculated for $\mathbf{L4}{\cdot}I_2$ and $(\mathbf{L4})_2{\cdot}I_2$ are very close (-7.3 and -7.6 kcal mol^{-1}, respectively), so that the formation of the latter adduct is only very slightly more favored as compared to that of the former, and electronic factors cannot be invoked as a reason for the exclusive isolation of the 2:1 CT adduct (see above).

As far as CT adducts are concerned, a Natural Population Analysis (NPA)[33] was undertaken aimed at evaluating the entity of the charge-transfer Q_{CT} occurring from the donors to dihalogens/interhalogens XY ($Q_{CT} = Q_I + Q_X$ for coordinated XY; Table 2). In the case of the hypothetical CT Se-adducts, the trend of Q_{CT} (Cl_2 > ICl ~ Br_2 > IBr > I_2) can be rationalized in terms of the absolute hardness η[34] calculated for dihalogens and interhalogens at the same level of theory (η = 2.67, 2.04, 2.15, 1.93, and 1.78 eV for Cl_2, ICl, Br_2, IBr, and I_2, respectively). The trend in Q_{CT} calculated for N-adducts is less easily interpreted, due to the lowest variability of Q_{CT} on varying the nature of the acceptor (Table 2).

Table 2. Donor to dihalogen/interhalogen, XY, Charge-Transfer Q_{CT} (|e|) calculated for 1:1 N- and Se- spoke adducts **L1**·XY and **L4**·XY (X = Y = Cl, Br, I; X = I, Y = Cl, Br) at the optimize geometries. In parentheses the absolute charge separation ΔQ_{XY} (|e|) within the coordinated dihalogen/interhalogen is reported.

	N-adducts	Se-adducts
$\mathbf{L1}{\cdot}Cl_2$	-0.164 (0.140)	-0.288 (0.072)
$\mathbf{L1}{\cdot}Br_2$	-0.168 (0.194)	-0.260 (0.092)
$\mathbf{L1}{\cdot}I_2$	-0.165 (0.233)	-0.212 (0.115)
L1·ICl	-0.166 (0.537)	-0.268 0.508)
L1·IBr	-0.155 (0.449)	-0.242 (0.320)
$\mathbf{L4}{\cdot}Cl_2$	-0.164 (0.152)	-0.305 (0.083)
$\mathbf{L4}{\cdot}Br_2$	-0.159 (0.209)	-0.275 (0.105)
$\mathbf{L4}{\cdot}I_2$	-0.157 (0.241)	-0.222 (0.130)
L4·ICl	-0.146 (0.670)	-0.279 (0.515)
L4·IBr	-0.137 (0.467)	-0.254 (0.330)

As expected, a remarkable increase in the calculated polarization of the interacting XY moiety is observed on passing from dihalogens ($\Delta Q_{XY} = |Q_X - Q_Y|$ in the range 0.140–0.233 |e|) to interhalogens (ΔQ_{XY} = 0.449 and 0.537 |e| for IBr and ICl for **L1** N-adducts; ΔQ_{XY} = 0.254 and 0.484 for free IBr and ICl in the gas phase, a similar trend is observed in the case of **L4**), indicating a progressive tendency to a limit $N{-}X^{+}{\cdots}Y^{-}$ structure along the series $Cl_2 < Br_2 < I_2$ < IBr < ICl, in agreement with the empirical observation that, as far as N···I–X

View Article Online
DOI: 10.1039/C8NJ00495A

systems are concerned, the N···I distances decrease with the increase of the electronegativity of the terminal atom (see above). Accordingly, in the series **L1**·I_2, **L1**·IBr, **L1**·ICl, Wiberg bond indices for the N···I interaction increase along the series (0.172, 0.215, and 0.253, respectively), while those of the interhalogen acceptor decrease (0.843, 0.787, and 0.722, respectively; Table S9 in ESI[†]), a similar trend is observed in the case of **L4**. More in general, it is noteworthy that the sums of bond indices calculated for the E···X and the X–Y systems (E = N and Se in spoke N-adducts and Se-adducts, respectively) amount to unity and are correlated to each other (Table S9 and Fig. S11 in ESI[†]), thus indicating that all the N···X–Y and Se···X–Y considered systems share a common nature of 3c-4e three body systems, independently on the nature of the halogen atomic species X and Y, in agreement with the analysis discussed above.

Conclusions

In this paper we report for the first time the reactivity towards dihalogens X_2 (X = Br, I) and interhalogens IX (X = Cl, Br) of donor molecules containing both nitrogen-heterocyclic and chalcogen donor sites, namely 2-arylselanyl pyridine derivatives **L1**-**L4**. The results in terms of structural diversity in the isolated products under the experimental conditions used, point out a clear preference for the formation of CT spoke N-adducts with I_2, IBr and ICl, which DFT calculations confirmed to be thermodynamically more stable than the 1:1 insertion adducts at the selenide Se-donor site. However, when strong oxidizing dihalogens such as Cl_2 and Br_2 are involved, Se-insertion adducts are the most favored products. The formation of CT spoke adducts implies the formation of a D···I─X halogen bond between the donor atom of a Lewis base (halogen bond acceptor) and the dihalogen acceptor (halogen bond donor). Therefore, when in the same molecule different donor sites can compete for the interaction with the same dihalogen acceptor, the formation of the halogen bond with one of the donor atom or the other can in principle be oriented and predicted, thus offering the possibility for molecular recognition events based on the formation of dihalogen CT spoke adducts.

Experimental

Materials and instruments. Reagents and solvents of reagent grade purity were used as received from Aldrich. The 2-arylselanyl pyridine derivatives **L1**-**L4** were prepared as previously described.[16]

The reactivity of **L1**-**L4** towards I_2, Br_2, ICl and IBr was tested in $CHCl_3$ and CH_3CN using a 1:1 donor-to-dihalogen/interhalogen molar ratio. Only in the case of **L4**, the reactivity towards I_2 was also tested using a 1:2 **L4**/I_2 molar ratio, but the isolated product resulted the same as that obtained by using a 1:1 molar ratio. Only for the synthesis reported below, solid products were isolated and single crystals suitable for X-ray diffraction analysis were successfully grown. From the reaction of **L4** with IBr in 1:1 molar ratio in CH_3CN, crystals of the pure ligand were obtained.

FT-Raman spectra (resolution ±4 cm^{-1}) were recorded on a Bruker RFS100 FTR spectrometer fitted with an indium–gallium arsenide detector (room temp) and operating with an excitation frequency of 1064 nm (Nd:YAG laser). The power level of the laser was tuned between 20–40 mW.

Synthesis of L1·I_2, L1·ICl, L1·IBr, $(L1)_{0.68}(L2)_{0.32}$·$I_{1.41}Cl_{0.59}$, L2·ICl, (L3)(L3H)I_3, $(L4)_2$·I_2, L4·2Cl_2, L4·Br_2: Title compounds were prepared from $CHCl_3$ or CH_3CN solutions of **L1**-**L4** and I_2, Br_2, ICl or IBr in 1:1 molar ratio by slow evaporation of the solvent at room temperature. In some cases, recrystallization was necessary in solvent mixtures.

L1·I_2: Prepared from **L1** (10.1 mg, 3.8 10^{-5} mol) and I_2 (9.64 mg, 3.8 10^{-5} mol) in $CHCl_3$ (2 mL). A red powder was isolated by slow evaporation of the solvent at room temperature; elemental analysis calcd. (%) for $C_{11}H_8ClI_2NSe$: C 25.29, H 1.54, N 2.68; found (%): C 25.27, H 1.52, N 2.70. Crystals suitable for X-ray diffraction analysis were grown from a CH_2Cl_2/CH_3CN (1/1 v:v) solution by slow evaporation at 4 °C. FT-Raman: ν = 164.8 s [ν(I–I)] cm^{-1}.

L1·ICl: Prepared from **L1** (5.7 mg, 2.1 10^{-5} mol) and ICl (3.4 mg, 2.1 10^{-5} mol, from a 1.48 10^{-2}M ICl stock solution in $CHCl_3$) in $CHCl_3$ (2 mL). Crystal were grown by slow evaporation of the solvent from the reaction mixture at room temperature; elemental analysis calcd. (%) for $C_{11}H_8Cl_2INSe$: C 30.66, H 1.87, N 3.25; found (%): C 30.64, H 1.85, N 3.27. FT-Raman: the decomposition of the compound even at low power levels of the laser made it difficult to assign the peaks related to the Se–I–Cl system.

L1·IBr: Prepared from **L1** (5.1 mg, 1.9 10^{-5} mol) and IBr (3.9 mg, 1.9 10^{-5} mol,) in $CHCl_3$ (2 mL). A yellow-orange powder was isolated by slow evaporation of the solvent at room temperature; elemental analysis calcd. (%) for $C_{11}H_8BrClINSe$: C 27.79, H 1.70, N 2.95; found (%): C 27.82, H 1.73, N 2.92. Crystals suitable for X-ray diffraction analysis were grown from a CH_2Cl_2/CH_3OH (1/1 v:v) solution by slow evaporation at 4 °C. FT-Raman: ν = 191.8 s, [ν(I–Br)] cm^{-1}.

$(\mathbf{L1})_{0.68}(\mathbf{L2})_{0.32}$·$I_{1.41}Cl_{0.59}$: Prepared from a 1:1 mixture of **L1**·I_2 (11.2 mg, 4.2 10^{-5} mol) and **L2**·ICl (17.41 mg, 4.2 10^{-5} mol) in CH_3CN (2.5 mL). Crystal were grown by slow evaporation of the solvent from the reaction mixture at room temperature; elemental analysis calcd. (%) for $C_{11}H_8Cl_{1.27}F_{0.32}I_{1.41}NSe$: C 28.53, H 1.74, N 3.02; found (%): C 28.52, H 1.70, N 3.00. FT-Raman: the decomposition of the compound even at low power levels of the laser made it difficult to assign the peaks related to the Se–I–Cl system.

L2·ICl: Prepared from **L2** (10.9 mg, 4.3 10^{-5} mol) and ICl (7.0 mg, 4.3 10^{-5} mol, from a 1.52 10^{-2}M ICl stock solution in CH_3CN) in CH_3CN (2.5 mL). Crystals were grown by slow evaporation of the solvent from the reaction mixture at room temperature; elemental analysis calcd. (%) for $C_{11}H_8ClFINSe$:

DOI: 10.1039/C8NJ00495A

C 31.88, H 1.95, N 3.38; found (%): C 31.85, H 1.93, N 3.40. FT-Raman: the decomposition of the compound even at low power levels of the laser made it difficult to assign the peaks related to the Se–I–Cl system.

(**L3**)(**L3**H)I_3: Prepared from **L3** (10.7 mg, 3.9 10^{-5} mol) and IBr (8.1 mg, 3.9 10^{-5} mol) in CH_3CN (2 mL). Crystal were grown by slow evaporation of the solvent from the reaction mixture at room temperature; elemental analysis calcd. (%) for $C_{22}H_{17}Cl_2I_3N_2Se_2$: C 28.76, H 1.86, N 3.05; found (%): C 28.74, H 1.87, N 3.03. FT-Raman: ν = 110.5 s, [ν_s(I–I–I)] cm^{-1}.

(**L4**)$_2$·I_2: Prepared from **L4** (10.1 mg, 2.6 10^{-5} mol) and I_2 (6.6 mg, 2.6 10^{-5} mol) in $CHCl_3$ (2 mL). Crystal were grown by slow evaporation of the solvent from the reaction mixture at room temperature; elemental analysis calcd. (%) for $C_{34}H_{26}I_2N_2Se_4$: C 39.56, H 2.54, N 2.72; found (%): C 39.55, H 2.52, N 2.75. FT-Raman: ν = 187.9 s [ν(I–I)] cm^{-1}.

L4·$2Cl_2$: Prepared from **L4** (9.0 mg, 2.3 10^{-5} mol) and ICl (3.7 mg, 2.3 10^{-5} mol, from a 1.48 10^{-2}M ICl stock solution in $CHCl_3$) in $CHCl_3$ (2 mL). A brownish powder was isolated by slow evaporation of the solvent at room temperature: elemental analysis calcd. (%) for $C_{17}H_{13}Cl_4NSe_2$: C 38.45, H 2.47, N 2.64; found (%): C 38.43, H 2.50, N 2.65. Crystals suitable for X-ray diffraction analysis were grown at room temperature by slow diffusion of *n*-hexane into a CH_2Cl_2 solution (during the crystallization the *n*-hexane phase turned purple). FT-Raman: ν = 265.5 br s [ν(I–I)] cm^{-1}.

L4·Br_2: Prepared from **L4** (10.4 mg, 2.7 10^{-5} mol) and Br_2 (4.3 mg, 2.7 10^{-5} mol, from a 6.9 10^{-2}M Br_2 stock solution in CH_3CN) in CH_3CN (1.5 mL). Crystal were grown by slow evaporation of the solvent from the reaction mixture at room temperature; elemental analysis calcd. (%) for $C_{17}H_{13}Br_2NSe_2$: C 37.19, H 2.39, N 2.55; found (%): C 37.21, H 2.37, N 2.57. FT-Raman: ν = 164.5 s [ν(I–I)] cm^{-1}.

X-ray crystallography. A summary of the crystal data and refinement details for the compounds discussed in this paper is given in Table S1 (ESI†). Diffraction data for **L4**, **L1**·$I_{1.41}Cl_{0.59}$ and (**L3**)(**L3**H)I_3 were collected at 120(2) K using mirror-monochromated Cu-*K*α *X*-radiation (λ = 1.54184 Å) and *ω* scans on a Rigaku Oxford Diffraction SuperNova Atlas four-circle diffractometer equipped with an Oxford Cryosystems open-flow cryostat. Diffraction data for **L1**·I_2, **L1**·ICl, **L1**·IBr, **L2**·ICl, (**L4**)$_2$·I_2, **L4**·$2Cl_2$ and **L4**·Br_2 were collected at 294(2) K using graphite-monochromated Mo-*K*α *X*-radiation (λ = 0.71073 Å) and *ω* scans on a Bruker APEX II CCD area detector diffractometer. All datasets were corrected for Lorentz and polarization effects and for absorption: empirical absorption correction using spherical harmonics, implemented in *CrysAlisPRO*[35] were applied to **L4**, **L1**·$I_{1.41}Cl_{0.59}$ and (**L3**)(**L3**H)I_3, whereas empirical absorption correction using SADABS[36] were applied to **L1**·I_2, **L1**·ICl, **L1**·IBr, **L2**·ICl, (**L4**)$_2$·I_2, **L4**·$2Cl_2$ and **L4**·Br_2. All the structures were solved by direct methods, and completed by iterative cycles of full-matrix least-squares refinement and Δ*F* syntheses using SHELXL-2014,[37] with non-hydrogen atoms refined with anisotropic displacement parameters. Hydrogen atoms were introduced at calculated positions and refined using a riding model. In (**L3**)(**L3**H)I_3 the N1'–H1' hydrogen atom was found in a difference Fourier map and thereafter refined freely.

During the early stages of the structure refinement of (**L1**)$_{0.68}$(**L2**)$_{0.32}$·$I_{1.41}Cl_{0.59}$ using a N–I–I model for the dihalogen moiety in the asymmetric unit, one of the sites showed an anomalous displacement parameter, thus suggesting that this site may be partially replaced by chlorine as indicated by micro-analytical data. A competitive refinement was carried out to investigate this possibility and a final model with a mixed-site I/Cl occupancy of 0.410(5)/0.590(5) was found to give the best fit to the data. A similar disorder was modelled for the halogen site on the aryl moiety of the donor ligand. A final model with a mixed-site Cl/F occupancy of 0.68(2)/0.32(2) was found to give the best fit to the data.

CSD 1588996-1589005 contain the supplementary crystallographic data for this paper. These data can be obtained free of charge from The Cambridge Crystallographic Data Centre *via* www.ccdc.cam.ac.uk/data_request/cif.

DFT Theoretical calculations. Theoretical calculations were performed at the DFT level[32] with the Gaussian 09 commercial suite of programs (rev. D.01)[38] on halogens X_2 (X = Cl, Br, I), interhalogen IX (X = Cl, Br), on the donors **L1** and **L4**, on the possible CT spoke N- and Se-adducts and the seesaw Se-adducts **L1**·IX and **L4**·IX, on the 2:1 CT N-adduct (**L4**)$_2$·I_2, and the 1:2 CT Se-adduct **L4**·$2Cl_2$. The mPW1PW hybrid functional[39] was adopted, along with Schäfer, Horn, and Ahlrichs double-ζ plus polarization all-electron basis sets (BS's) on C, N, and H. For halogen and selenium atomic species,[40] the LanL08d BS's with relativistic effective core potentials (RECPs)[41] were employed, providing d-type polarization functions.[42] The molecular geometry optimizations were performed starting from structural data, when available. Tight SCF convergence criteria (SCF = tight keyword) and fine numerical integration grids [Integral(FineGrid) keyword] were used. The nature of the minima for the corresponding optimized structures were verified by harmonic frequency calculations. Thermochemical data, including Zero Point Energy corrections, were calculated at the same level of theory. Basis Set Superposition Errors were evaluated for model systems (**L1** and **L4** CT N- and Se-adducts with I_2 and ICl) and were found in all cases negligible, not exceeding 1.6 kcal mol^{-1} in the case of the 1:1 N-adduct **L1**·I_2). Natural atomic charges,[43] and Wiberg bond indexes were calculated at the optimized geometries at the same level of theory. The absolute charge transfer Q_{CT} and the polarization Q_{IX} of free and coordinated halogens and interhalogens were calculated from natural charges. Although Koopmans's theorem does not apply to DFT, absolute hardness values η were calculated for the considered dihalogens and interhalogens from the Kohn-Sham eigenvalues calculated for HOMO and LUMO according to Pearson's definition.[34] The programs GaussView 5[43] and Molden 5.2[44] were used to investigate the optimized structures and molecular orbital shapes.

Acknowledgements

View Article Online
DOI: 10.1039/C8NJ00495A

The authors thank Università degli Studi di Cagliari, FAPERGS, CNPq, and CAPES for financial support. CNPq is also acknowledged for the fellowship for G.P., and E.J.L. This manuscript is part of the scientific activity of the international multidisciplinary "SeS Redox and Catalysis" network.

† Electronic supplementary information (ESI) available: Additional information as noted in the text including: crystallographic data for the compounds **L1**·I$_2$, **L1**·ICl, **L1**·IBr, (**L1**)$_{0.68}$(**L2**)$_{0.32}$·I$_{1.41}$Cl$_{0.59}$, **L2**·ICl, (**L3**)(**L3**H)I$_3$, (**L4**)$_2$·I$_2$, **L4**·2Cl$_2$, **L4**·Br$_2$; selected calculated bond distances for the optimized structures, ball and stick representations of the optimized structures; CCDC 1588996-1589005 contain the supplementary crystallographic data for this paper. For ESI and crystallographic data in CIF or other electronic format see DOI: 10.1039/…….

[a] Dipartimento di Scienze Chimiche e Geologiche, Università degli Studi di Cagliari, S.S. 554 Bivio per Sestu 09042 Monserrato (CA), Italy. E-mail lippolis@unica.it, aragoni@unica.it.
[b] School of Chemistry, University of Nottingham, Nottingham, BG72RD UK.
[c] Dipartimento di Chimica, Università degli Studi di Milano, via Golgi 19, 20133 Milano, Italy.
[d] Laboratório de Síntese Orgânica Limpa-LASOL, CCQFA, Universidade Federal de Pelotas – UFPel, PO Box 354, 96010-900 Pelotas, RS, Brazil.

1. (a) M. Arca, F. Demartin, F.A. Devillanova, A. Garau, F. Isaia, V. Lippolis and G. Verani, *Trends in Inorg. Chem*., 1999, **6**, 1-18; (b) P. D. Boyle, S. M. Godfrey, *Coord. Chem. Rev*., 2001, **223**, 265-299 (c) A. Garau, F. Isaia, V. Lippolis, A. Mancini and G. Verani, *Bioinorg. Chem. Appl*., 2006, **1**, 1-12.
2. (a) M. C. Aragoni, M. Arca, F. Demartin, F.A. Devillanova, A. Garau, F. Isaia, F. Lelj, V. Lippolis and G. Verani, *Chem. Eur. J.*, 2001, **7**, 3122-3133; (b) E. J. Juárez-Pérez, M. C. Aragoni, M. Arca, A. J. Blake, F. A. Devillanova, A. Garau, F. Isaia, V. Lippolis, R. Núñez, A. Pintus and C. Wilson, *Chem. Eur. J.*, 2011, **17**, 11497-11514.
3. (a) W. T. Pennington, T. W. Hanks, and H. D. Arman, *Struct. Bonding*, 2008, **126**, 65-104; (b) V. Lippolis, F. Isaia in *Handbook of Chalcogen Chemistry: New Perspectives in Sulfur, Selenium and Tellurium (2nd Edition)*, F.A. Devillanova, W.-W. du Mont (Ed.s), RSC Publishing, 2013, Part 1, Chapter 8.2, 448-472; (c) M. Arca, F. Demartin, F.A. Devillanova, A. Garau, F. Isaia, V. Lippolis and G. Verani, *J. Chem. Soc., Dalton Trans.*, 1999, 3069-3073; (d) W.-W. du Mont, M. Bätcher, C. Daniliuc, F. A. Devillanova, C. Druckenbrodt, J, Jeske, P. G. Jones, V. Lippolis, R. Futhe and E. Seppälä, *Eur. J. Inorg. Chem.*, 2008, **29**, 4562-4577.
4. W. Nakanishi, S. Hayashi, M. Hashimoto, M. Arca, M. C. Aragoni, V. Lippolis *in PATAI's Chemistry of Functional Groups, "The Chemistry of Organic Selenium and Tellurium Compounds"*, Zvi Rappoport Ed., Wiley 2013, Vol. 4, part 2, pp 885-972.
5. R. Núñez, P. Farràs, F. Teixidor, C. Viñas, R. Sillanpää, R. Kivekäs, *Angew. Chem. Internat. Ed.*, 2006, **45**, 1270-1272.
6. R. B. Walsh, C. W. Padgett, P. Metrangolo, G. Resnati, T. W. Hanks, W. T. Pennington, *Crystal Growth & Design*, 2001, **1** (2), 165–175.
7. (a) A. Mancini, M.C. Aragoni, N. Bricklebank, C. Castellano, F. Demartin, F. Isaia, V. Lippolis, A. Pintus, M. Arca, *Chem. Asian J.*, 2013, **8**, 639–647; (b) Y.V. Torubaev, I.V. Skabitskiy, A.V. Pavlova, A.A. Pasynskii, *New J. Chem.*, 2017, 41, 3606-3611; (c) R. Montis, M. Arca, M.A. Aragoni, A. Bauzá, F. Demartin, A. Frontera, F. Isaia, V. Lippolis, *CrystEngComm*, 2017, **19**, 4401-4412.
8. (a) F. Isaia, M. C. Aragoni, M. Arca, F. Demartin, F. A. Devillanova, G. Floris, A. Garau, M. B. Hursthouse, V. Lippolis, R. Medda, F. Oppo and G. Verani, *J. Med. Chem.*, 2008, **5**, 4050-4053; (b) C. Raby, J. F. Lagorce, A. C. Jambut-Absil, J. Buxeraud and G. Catanzano, *Endocrinology*, 1990, **126**, 1683-1691; (c) G. Roy, K. P. Bhabak and G. Mugesh, *Cryst.GrowthDes.* 2011, **11**, 2279-2286; (d) Vengurlekar S., Sharma R. and Trivedi P. *Letters in Drug Design and Discovery,* 2012, **9**, 549-555; (e) D. H. Mahajan, K. H. Chikhalia, C. Pannecouque and E. De Clercq, *Pharm. Chem. J.,* 2012, **46**, 165-170; (f) M. M. Ghanbari, G. H. Mahdavinia, J. Safari, H. Naeimi and M. Zare *Synth. Comm.*, 2011, **41**, 2414-2420; (g) A. D. Jangale, Y. B. Wagh, Y. A. Tayade and D. S. Dalal, *Synth.Comm.*, 2015, **45**, 1876-1886; (h) H. Tavakol, T. Hadadi and H. Roohi, *J. of Struct. Chem.*, 2012, **53**, 649-658; (i) M. C. Aragoni, M. Arca, F. Demartin, F. A. Devillanova, A. Garau, F. Isaia,V. Lippolis, and G. Verani, *J. Am. Chem. Soc.*, 2002, **124**, 4538-4539.
9. V. Lippolis in *Organoselenium Compounds in Biology and Medicine: Synthesis, Biological and Therapeutic Treatments*, V. K. Jain and K. I. Priyadarsini (Eds.), RSC Publishing 2017, Cambridge, Chapter 4, pp. 122-149.
10. E. L. Rimmer, R. D. Bayley, W. T. Pennington, T. W. Hanks, *J. Chem. Soc.. Perkin Trans.*, 1998, 2, 2557.
11. M. C. Aragoni, M. Arca, F. A. Devillanova, M. B. Hursthouse, S. L. Huth, F. Isaia, V. Lippolis, A. Mancini, G. Verani, *J. Organomet. Chem.,* 2005, **690**, 1923-1934.
12. M. C. Aragoni, M. Arca, F. A. Devillanova, M. B. Hursthouse, S. L. Huth, F. Isaia, V. Lippolis, A. Mancini, *Chem. Commun*., 2004, **6**, 540-542.
13. M. C. Aragoni, M. Arca, F. A. Devillanova, M. B. Hursthouse, S. L. Huth, F. Isaia, V. Lippolis, A. Mancini, H. Ogilvie, *Inorg. Chem. Commun.,* 2005, **8**, 79-82.
14. M. C. Aragoni, M. Arca, F. A. Devillanova, M. B. Hursthouse, S. L. Huth, F. Isaia, V. Lippolis, A. Mancini, G. Verani, *Eur. J. Inorg. Chem.,* 2008, 3921-3928.
15. M. C. Aragoni, M. Arca, S. J. Coles, F. A. Devillanova, M. B. Hursthouse, S. L. Coles née Huth, F. Isaia, V. Lippolis, A. Mancini, *CrystEngComm,*2011, **13**, 6319-6322.
16. S. Thurow, R. Webber, G. Perin, E.J. Lenardão, D. Alves, *Tetrahedron Lett.,* 2013, **54**, 3215-3218.
17. M. Arca, F.A. Devillanova, A. Garau, F. Isaia, V. Lippolis, G. Verani, *Z. anorg. allg. Chem*., 1998, **624**, 745-749.
18. C. Janiak, *J. Chem. Soc., Dalton Trans.*, 2000, 3885–3896.
19. (a) I. Caracelli, J. Zukerman-Schpector and E.R. T. Tiekink, *Coord.Chem.Rev*., 2012, **256**, 412– 438; (b) I. Caracelli, J. Zukerman-Schpector, I. Haiduc, E.R. T. Tiekink, *CrystEngComm*, 2016, **18**, 6960–6978.
20. (a) A. Bondi, *J. Phys. Chem.*, 1964, **68** (3), 441–451; (b) S. Alvarez, *Dalton Trans.*, 2013, **42**, 8617–8636.
21. M.C. Aragoni, M. Arca, F. Demartin, F.A. Devillanova, T. Gelbrich, A. Garau, M.B. Hursthouse, F. Isaia, V. Lippolis, *Crystal Growth & Design*, 2007, **7**, 1284-1290.
22. G. A. Landrum, N. Goldberg and R. Hoffmann *J. Chem. Soc. Dalton Trans.*, 1997, 3605-3613.
23. G. R. Desiraju, P. S. Ho, L. Kloo, A. C. Legon, R. Marquardt, P. Metrangolo, P. Politzer, G. Resnati and K. Rissanen, *Pure Appl. Chem.*, 2013, **85**, 1711-1713.
24. L. P. Wolters, P. Schyman, M. J. Pavan, W. L. Jorgensen, F.M. Bickelhaupt and S. Kozuch, *WIREs Comput. Mol. Sci.*, 2014, **4**, 523-540.
25. C. Wang, D. Danovich, Y. Mo and S. Shaik, *J. Chem. Thery and Comput.*, 2014, **10**, 3726-3737.
26. A. Bauzá, D. Quiñonero, P. M. Deyà and A. Frontera, *CrystEngComm*, 2013, **15**, 3137-3144.
27. (a) R. J. Hach and R. E. Rundle, *J. Am. Chem. Soc*., 1951, **73**, 4321-4324; (b) C. G. Pimentel, *J. Chem. Phys*., 1951, **19**, 446-448.
28. M. C. Aragoni, M. Arca, F. A. Devillanova, F. Isaia and V. Lippolis, *Cryst. Growth Des.*, 2012, **12**, 2769–2779. For an A-B-C three body system the relative elongation are calculated according the following equations were r_{cov} are the covalent raddii of the relevant atoms: $\delta_{AB} = \frac{d_{AB}-(r_{cov}A+r_{cov}B)}{r_{cov}A+r_{cov}B}$; $\delta_{BC} = \frac{d_{BC}-(r_{cov}B+r_{cov}C)}{r_{cov}B+r_{cov}C}$
29. (a) Ciancaleoni, M. Arca, G. F. Caramori, G. Frenking, F. S. S. Schneider and V. Lippolis *Eur. J. Inorg. Chem.*, 2016, 3804–3812, (b)
30. F. Isaia, M.C. Aragoni, M. Arca, F. Demartin, F. A. Devillanova, G. Ennas, A. Garau, V. Lippolis, A. Mancini, G. Verani, Eur. J. Inorg.Chem., 2009, 3667.

View Article Online
DOI: 10.1039/C8NJ00495A

31. F. van Bolhuis, P.B. Koster, T. Migchelsen, *Acta Crystallographica.*1967, **23**(1):90–91.
32. W. Koch and M. C. Holthausen, *A Chemist's Guide to Density Functional Theory*, Wiley-VCH, Weinheim, Germany, 2nd edn, 2002.
33. Reed, A. E.; Weinstock, R. B.; Weinhold, F. *J. Chem. Phys.,* 1985, **83**, 735–746.
34. R. G. Pearson, *J. Am. Chem. Soc.*, 1985, **107**, 6801–6806.
35. *CrysAlis PRO*. Rigaku Oxford Diffraction, Yarnton, Oxfordshire, England, 2014.
36. G.M. Sheldrick, *SADABS* Area-Detector Absorption Correction Program, Bruker AXS Inc., Madison, Wisconsin, USA, 2000.
37. G. M. Sheldrick, *Acta Crystallogr., Sect. C* 2015, **71**, 3–8.
38. Gaussian 09 rev. D.01, M. J. Frisch, G. W. Trucks, H. B. Schlegel, G. E. Scuseria, M. A. Robb, J. R. Cheeseman, G. Scalmani, V. Barone, B. Mennucci, G. A. Petersson, H. Nakatsuji, M. Caricato, X. Li, H. P. Hratchian, A. F. Izmaylov, J. Bloino, G. Zheng, J. L. Sonnenberg, M. Hada, M. Ehara, K. Toyota, R. Fukuda, J. Hasegawa, M. Ishida, T. Nakajima, Y. Honda, O. Kitao, H. Nakai, T. Vreven, J. A. Montgomery, Jr., J. E. Peralta, F. Ogliaro, M. Bearpark, J. J. Heyd, E. Brothers, K. N. Kudin, V. N. Staroverov, T. Keith, R. Kobayashi, J. Normand, K. Raghavachari, A. Rendell, J. C. Burant, S. S. Iyengar, J. Tomasi, M. Cossi, N. Rega, J. M. Millam, M. Klene, J. E. Knox, J. B. Cross, V. Bakken, C. Adamo, J. Jaramillo, R. Gomperts, R. E. Stratmann, O. Yazyev, A. J. Austin, R. Cammi, C. Pomelli, J. W. Ochterski, R. L. Martin, K. Morokuma, V. G. Zakrzewski, G. A. Voth, P. Salvador, J. J. Dannenberg, S. Dapprich, A. D. Daniels, O. Farkas, J. B. Foresman, J. V. Ortiz, J. Cioslowski, and D. J. Fox, Gaussian, Inc., Wallingford CT, **2013**.
39. C. Adamo, V. Barone, *J. Chem. Phys.*, 1998, **108**, 664-675.
40. F. Weigend and R. Ahlrichs, *Phys. Chem. Chem. Phys*., 2005, **7**, 3297.
41. T.H. Dunning Jr. and P.J. Hay, in *Methods of Electronic Structure Theory*, ed. H. F. Schaefer III, Plenum Press, New York, vol. 2, 1977.
42. L. E. Roy, P. J. Hay and R.L. Martin, *J. Chem. Theory Comput*., 2008, **4**, 1029-1031.
43. GaussView 5.0.9, R. Dennington, T. Keith, and J. Millam, Semichem Inc., Shawnee Missouri, KS, 2009.
44. G. Schaftenaar and J. H. Noordik, *J. Comput.-Aided Mol. Des.*, 2000, **14**, 123.

DOI: 10.1039/C8NJ00495A

Graphycal Abstract

Structural diversity in the products formed by the reactions of 2-arylselanyl pyridine derivatives and dihalogens†

R. Montis, M. Arca, M. C. Aragoni, A. J. Blake, C. Castellano, F. Demartin, F. Isaia, V. Lippolis, A. Pintus, E. J. Lenardão, G. Perin, A. E. O'Connor, S. Thurow

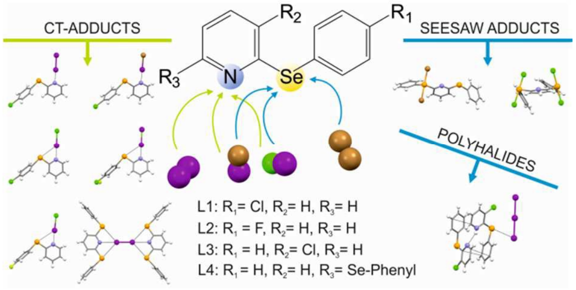

The simultaneous presence of competing donor sites in L1-L4 influences their reactivity towards dihalogens and interhalogens: A halogen bond hierarchy study.